Interaction-induced topological superconductivity in antiferromagnet-superconductor junctions

Senna S. Luntama,[1] Päivi Törmä,[1] and Jose L. Lado[1,*]

[1]Department of Applied Physics, Aalto University, 00076 Aalto, Espoo, Finland

(Dated: February 23, 2021)

We predict that junctions between an antiferromagnetic insulator and a superconductor provide a robust platform to create a one-dimensional topological superconducting state. Its emergence does not require the presence of intrinsic spin-orbit coupling nor non-collinear magnetism, but arises solely from repulsive electronic interactions on interfacial solitonic states. We demonstrate that a topological superconducting state is generated by repulsive interactions at arbitrarily small coupling strength, and that the size of the topological gap rapidly saturates to the one of the parent trivial superconductor. Our results put forward antiferromagnetic insulators as a new platform for interaction-driven topological superconductivity.

The search for topological superconductors has been one of the most active areas in condensed matter physics in recent years[1–19]. These systems, pursued in particular for the emergence of Majorana zero modes, represent one of the potential solid state platform for the implementation of topological quantum computing[20,21]. Due to their elusive nature, topological superconductors are often artificially engineered. A variety of platforms have been proposed and demonstrated for this purpose[17,22,23], generically relying on a combination of conventional s-wave superconductivity, ferromagnetism and strong spin-orbit coupling[7–10,15,24,25].

While ferromagnets have played a central role for artificial topological superconductivity, antiferromagnetic insulators have been overlooked for this purpose. Recently, antiferromagnets have attracted a great amount of attention due to their unique properties for spintronics[26–30] and for creating novel types of topological matter[31–37]. Ferromagnetism efficiently lifts Kramer's degeneracy, a process heavily detrimental for spin-singlet superconductivity. Antiferromagnetism, in comparison, does not lift Kramer's degeneracy between opposite spins in the absence of spin-orbit coupling, a feature that could potentially make antiferromagnetism more compatible with spin-singlet superconductivity.[38–45].

Here we show that two-dimensional topologically trivial antiferromagnetic insulators provide a platform to design one-dimensional topological superconductivity. In our proposal, spin-orbit coupling effects are not necessary for topological superconductivity to appear, nor a fine-tuning between the different components of the system. In contrast, we show that long-range interactions alone give rise to a non-trivially gapped state hosting Majorana excitations, and that the interaction-induced gap opening is topological irrespective of details. We demonstrate that the robustness of this unique state stems from the solitonic nature of the emergent excitations at the interface, in which interaction-induced gap opening unavoidably gives rise to a topological superconducting state. Our results put forward antiferromagnet-superconductor junctions as a robust platform to engineer interaction-induced topological superconductivity.

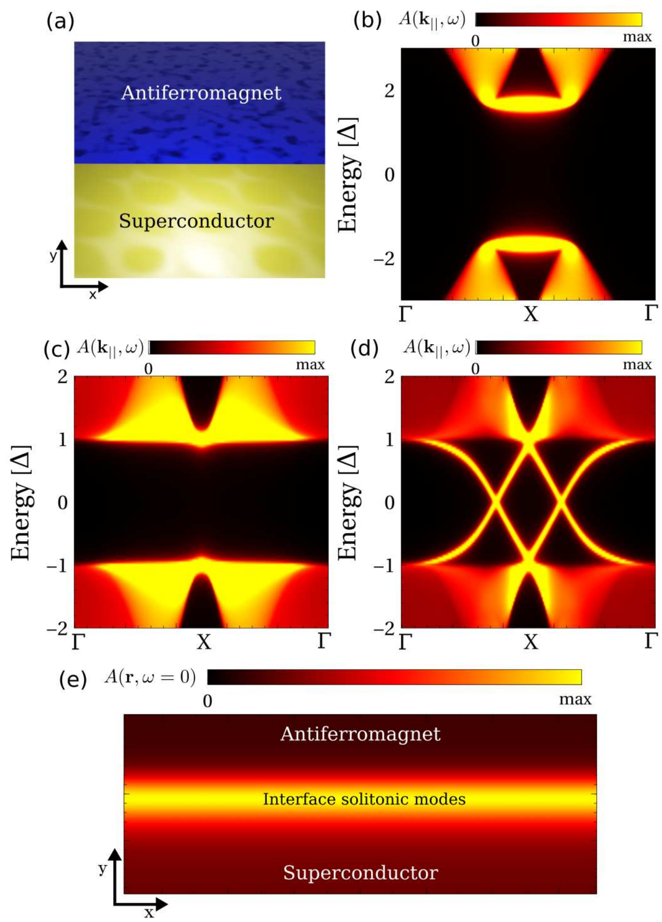

FIG. 1. (a) A sketch of the two dimensional antiferromagnet (AF) and superconductor (SC) forming a one-dimensional AF-SC interface. The spectral function at the surface of the AF (b), at the surface of the SC (c) and at the interface between AF and SC (d) as given by our model Hamiltonian (1) in a honeycomb lattice. Panel (e) shows the spatial distribution of the interfacial modes. Here we chose $\Delta = 0.3t$, $m_{\mathrm{AF}} = 0.5t$, $\mu = t$ and $V_1 = V_2 = 0$.

Our system consists of a junction between a conventional s-wave superconductor and antiferromagnetic insulator, as shown in Fig. 1a. To model this system, we take a Hamiltonian in the honeycomb lattice of the form

$$\mathcal{H} = \mathcal{H}_{\text{kin}} + \mathcal{H}_{\text{AF}} + \mathcal{H}_{\text{SC}} + \mathcal{H}_{\text{int}} \tag{1}$$

where

$$\mathcal{H}_{\text{kin}} = t \sum_{\langle ij \rangle, s} c^\dagger_{i,s} c_{j,s} + \sum_{i,s} \mu(\mathbf{r}_i) c^\dagger_{i,s} c_{i,s} \tag{2}$$

$$\mathcal{H}_{\text{AF}} = \sum_{i,s} m_{\text{AF}}(\mathbf{r}_i) \tau^z_{i,i} \sigma^z_{s,s} c^\dagger_{i,s} c_{i,s} \tag{3}$$

$$\mathcal{H}_{\text{SC}} = \sum_{i} \Delta(\mathbf{r}_i) c_{i,\uparrow} c_{i,\downarrow} + \text{H.c.} \tag{4}$$

$$\begin{aligned}\mathcal{H}_{\text{int}} = V_1 \sum_{\langle ij \rangle} \left(\sum_s c^\dagger_{i,s} c_{i,s} \right) \left(\sum_s c^\dagger_{j,s} c_{j,s} \right) + \\ V_2 \sum_{\langle\langle ij \rangle\rangle} \left(\sum_s c^\dagger_{i,s} c_{i,s} \right) \left(\sum_s c^\dagger_{j,s} c_{j,s} \right)\end{aligned} \tag{5}$$

where $c^\dagger_{i,s}$ is the fermionic creation operator for site i and for spin s, σ^z denotes the spin Pauli matrix, τ^z the sublattice Pauli matrix, $\langle\rangle$ the first neighbors and $\langle\langle\rangle\rangle$ the second neighbors. Taking that the interface between the antiferromagnet and the superconductor is located at $\mathbf{r} = (x, 0, 0)$ we take $\Delta(\mathbf{r}) = \frac{\Delta}{2}[1 - \text{sign}(y)]$ $\mu(\mathbf{r}) = \frac{\mu}{2}[1 - \text{sign}(y)]$ and $m_{\text{AF}}(\mathbf{r}) = \frac{m_{\text{AF}}}{2}[1 + \text{sign}(y)]$[46]. The repulsive interaction term of Eq. 5 is solved at the mean-field level including the usual mean-field decouplings $\mathcal{H}_{\text{int}} \approx \mathcal{H}^{\text{MF}} = \sum \chi_{ijss'} c^\dagger_{i,s} c_{j,s'}$ with $\chi_{ijss'}$ the self-consistent mean-field parameters[47]. On-site interactions are incorporated in $m_{\text{AF}}(\mathbf{r})$ and $\Delta(\mathbf{r})$ at the mean-field level.

It is instructive to examine the electronic bandstructure in the absence of interactions and in the absence of an interface. Let us consider a semi-infinite slab in the $y-$direction, having translational symmetry in the $x-$direction as depicted in Fig. 1a. For that geometry, we compute the momentum-resolved spectral function at the edge $A(\mathbf{k}_{||}, \omega) = -\frac{1}{\pi} \text{Im} \left(\omega - \mathcal{H}(\mathbf{k}_{||}) + i0^+ \right)^{-1}$ using the Dyson formalism[48]. For both isolated superconductor and antiferromagnet, the surface spectral function presents a gap, as shown in in Fig. 1bc, that simply stems from the gapped topologically trivial band structure. In the case of the superconductor the gap is controlled by Δ, whereas in the antiferromagnet, the gap is determined by m_{AF}. In stark contrast, when the antiferromagnet and superconductor are joined together, a new branch of interfacial modes appear as shown in Fig. 1d. By computing the spectral function in real space at zero energy $A(\mathbf{r}, \omega = 0)$ it is clearly seen that the new branch is heavily localized at the junction between the superconductor and the antiferromagnet. We have verified, that for different values of the superconducting and antiferromagnet order parameters, zero modes emerge as long as the order parameters are not substantially bigger than the typical bandwidth.

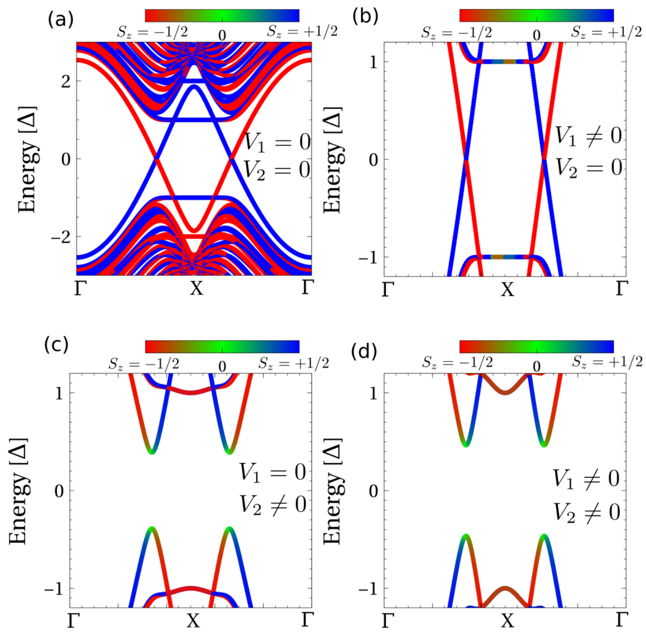

FIG. 2. (a) Non-interacting bands in a ribbon geometry. First neighbor interactions do not lead to a gap (b), whereas second neighbor interactions drive a gap opening (c). When both first and second neighbor interactions are present the gap remains. The parameters are $V_1 = t$ in (b), $V_2 = 1.7t$ in (c) $V_1 = t$ $V_2 = 2t$ in (d) and $m_{AF} = 0.8t$ $\Delta = 0.4t$ in (a-d).

The emergence of the interfacial zero modes can be rationalized from a low energy model for the honeycomb lattice[49–53]. For the following analytic derivation, it is convenient to take $\mu = 0$ so that the full antiferromagnet-superconductor can be described with a generalized Dirac equation at the K point of the honeycomb lattice[54]. The low energy excitations can be captured by an effective model around the valleys $\mathcal{V}^z = \pm 1$, and we will focus first on taking the momentum parallel to the interface $p_x = 0$. By defining the Nambu spinor $\Psi^\dagger = (c^\dagger_{A,\uparrow,\mathbf{k}}, c^\dagger_{B,\uparrow,\mathbf{k}}, c_{A,\downarrow,-\mathbf{k}}, c_{B,\downarrow,-\mathbf{k}})$, the Hamiltonian in the electron-up/hole-down sector ($\Uparrow$) can be written as $\mathcal{H}(p_x = 0, p_y)_\kappa = \frac{1}{2} \Psi^\dagger H_\kappa \Psi$ with

$$H_\kappa = \begin{pmatrix} m_{\text{AF}}(\mathbf{r}) & p_y & \Delta(\mathbf{r}) & 0 \\ p_y & -m_{\text{AF}}(\mathbf{r}) & 0 & \Delta(\mathbf{r}) \\ \Delta(\mathbf{r}) & 0 & m_{\text{AF}}(\mathbf{r}) & -p_y \\ 0 & \Delta(\mathbf{r}) & -p_y & -m_{\text{AF}}(\mathbf{r}). \end{pmatrix} \tag{6}$$

The spectrum of this effective model is gapped at $y \pm \infty$, as expected from its asymptotic antiferromagnet/superconductor gap. However, a zero energy mode $H|\psi_\Uparrow\rangle = 0$ at the interface can be always built, taking the functional form $\psi^\dagger_\Uparrow = e^{-\int_0^y [\Delta(y')-m_{\mathrm{AF}}(y')]dy'}(c^\dagger_{A,\uparrow}+ic^\dagger_{B,\uparrow}-ic_{A,\downarrow}-c_{B,\downarrow})$. The nature of this zero mode is analogous to the Jackiw-Rebbi soliton[49], and therefore can be understood as an antiferromagnet-superconducting soliton. The complementary electron-down/hole-up ($\Downarrow$) sector of the Hamiltonian will therefore also host a zero mode, that we label as $\psi_\Downarrow$. Away from the point $p_x = 0$, the previous state acquires a finite dispersion given by first order perturbation theory $v_F p_x = \langle \psi_\Uparrow | \mathcal{H} | \psi_\Uparrow \rangle$. As a result, close to the K-points two branches of zero modes appear, giving rise to the effective low energy Hamiltonian

$$H(p_x) = \sum_\kappa v_F p_x \mathcal{V}^z_{\kappa,\kappa}[\psi^\dagger_{\Uparrow,\kappa,p_x}\psi_{\Uparrow,\kappa,p_x} - \psi^\dagger_{\Downarrow,\kappa,p_x}\psi_{\Downarrow,\kappa,p_x}] \tag{7}$$

where κ runs over the two valleys. It is interesting to note that the four modes are not independent, but they are related by electron-hole symmetry operator $\Xi = \theta^y \sigma^y \mathcal{C}$ with θ^y the Nambu Pauli matrix and $\mathcal{C}$ complex conjugation as $\Xi^{-1}\psi_{\Uparrow,+1,p_x}\Xi = \psi_{\Downarrow,-1,-p_x}$ due to the built-in Nambu electron-hole symmetry of the Hamiltonian. Therefore, the Hamiltonian Eq. 7 hosts only two physical degrees of freedom, each one propagating in opposite directions, realizing an effective spinless one-dimensional model. These singly-degenerate channels are analogous to quantum Hall edge states[15], and helical channels in topological insulators[7], states that provide a starting point for engineering a topological superconducting gap. Remarkably in our case, as will be shown below, the solitonic gapless channels will open up a topological superconducting gap once electron-electron interaction effects are included.

Let us now move on to consider the impact of long-range electronic interactions in the solitonic modes. For computational convenience, we now perform our calculations in ribbons of finite width in the x-direction, in which we take the transverse direction wide enough to avoid finite-size effects. The previous gapless interface modes of Fig. 1d and derived in Eq. 7 appear in this ribbon geometry as shown in Fig. 2a, where $S_z = \frac{1}{2}\langle \sum_{n,s} \sigma^z_{s,s} c^\dagger_{n,s} c_{n,s} \rangle_{\Psi_k}$ with Ψ_k the eigenstate. It is shown that in the absence of interactions, the sectors $S_z = \pm 1/2$ are fully decoupled, stemming from the $U(1)$-spin symmetry of the Hamiltonian. With this lattice model, we now explore the impact of electronic interactions by solving self-consistently Eq. 1. Note that the interactions apply both along the interface and across it. We start by considering only first neighbor interactions, taking $V_2 = 0$. In this situation, a gap does not open even when V_1 is increased, as shown in Fig. 2b. We now move on to the case of V_2, taking first $V_1 = 0$. As observed in Fig. 2c, it is clearly seen that now a gap opens up. This behavior also takes place when V_1 is taken to be non-zero, see Fig. 2d. As a result, second neighbor interactions are the only interaction capable of opening up a gap on the topological interface modes, whose magnitude is marginally affected by the first neighbor interactions.

The emergence of a gap opening driven by electronic interactions raises the question of potential non-trivial topological properties. From the point of view of the effective low energy model, interactions create an effective term in Eq. 7 of the form $H^{MF} \sim \langle \Psi_\Uparrow \Psi^\dagger_\Downarrow \rangle \Psi^\dagger_\Uparrow \Psi_\Downarrow$+H.c.. It is interesting to note that due to the solitonic functional form of $\Psi_\Uparrow$ and $\Psi_\Downarrow$ and their relation via electron-hole symmetry, the gap ($\propto \langle \Psi_\Uparrow \Psi^\dagger_\Downarrow \rangle$) created is odd with respect to κ, the valley index, suggesting the emergence of an effective topological superconducting state. To verify the non-trivial topological nature of the interaction-driven gapped state, we compute both its Z_2 topological invariant[1,55] and surface spectral function. We revealed that the gapped system has a topologically non-trivial Z_2 invariant, signaling the existence of a topological superconducting state. This is further verified when computing the density of states at the edge of the interface in a ribbon that spans from $x = 0$ to $x = \infty$, as shown in Fig. 3a. The edge of the system hosts a zero-mode resonance associated with the unpaired Majorana stemming from the non-trivial electronic structure. This is contrasted with the finite gap present in the bulk of the system shown in Fig. 3b. The localization of the zero-mode can also be seen when computing the spectral function for $\omega = 0$, Fig. 3c.

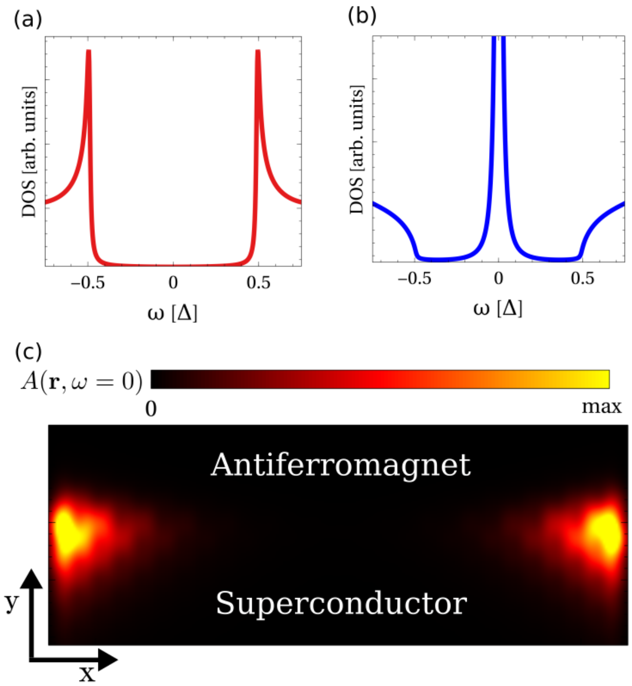

FIG. 3. (a) Spectral function in the bulk in the presence of interactions, and (b) at the edge showing the emergence of a zero Majorana mode. Panel (c) shown the spectral function at $\omega = 0$ for a finite junction, featuring edge zero Majorana modes. We used now $\Delta = 0.4t$, $m_{\mathrm{AF}} = 0.8t$, $V_1 = t$ and $V_2 = 2t$.

Let us now move on to look at the impact of long-range interactions, and in particular, at the interplay between the first and second neighbor interactions at the mean field level. For the sake of simplicity in the following discussion we will only consider effects that appear by means of a mean field decoupling of Eq.5, without considering beyond mean-field effects or additional $t-J$ contributions. At the mean-field level, the interaction term of Eq. 5 can give rise to two potential effects: first, interaction induced hoppings and second, symmetry broken states such as charge density waves. In the weak coupling regime considered here, only interaction-induced hopping terms arise. In particular, the time-reversal symmetric and spin-dependent part of $\chi_{ijss'}$ yield an effective spin and spatially-dependent synthetic spin-orbit coupling term of the Kane-Mele form[7,56]. This interaction-induced term creates spin-mixing in the solitonic modes, opening up a topological gap.

The interplay of first and second neighbor interactions can be easily rationalized within this language. From the mean-field point of view, first neighbor interactions can give rise to interaction induced Rashba spin-orbit coupling terms[57], whereas second neighbor interactions can give rise to interaction-induced Kane-Mele spin-orbit coupling[58]. However, due to valley polarized nature of the solitonic modes, interaction induced Rashba-spin-orbit coupling does not open up a gap in them[57], whereas Kane-Mele like spin-orbit[58] can create a gap. As a result, second neighbor interactions are the only ones capable of interaction-induced gap opening in the system. In contrast, the effect of the first neighbor interactions is to simply create a Fermi velocity renormalization[59,60] increasing the kinetic energy of the solitonic modes, yet without any competing mechanism for gap opening.

It is crucial to understand whether the gap opening requires a finite minimum value of interaction strength. We investigate this by taking the first neighbor interaction $V_1 = 0$, and looking at the topological gap as a function of the repulsive second neighbor interaction V_2. It is clearly observed that the topological gap becomes stronger as V_2 is increased, without the existence of a critical value for the transition (Fig. 4a). In particular, a logarithmic plot of the gap (inset of Fig. 4a) at small coupling strength reveals that the topological gap δ follows an exponential dependence $\delta \sim e^{-\frac{v_F}{V_2}}$[61]. Interestingly, whereas exponential dependences of that form are typical for superconducting instabilities driven by attractive interactions[62], in our present case interactions are actually repulsive. This behavior stems from the projection of the interactions in the low energy solitonic model of Eq. 7, driving a topological phase transition at arbitrarily small couplings. At large coupling strengths V_2, the topological gap saturates to the gap of the superconductor. This behavior should be contrasted with the other schemes proposed for topological superconductivity, in which the topological gap is usually substantially smaller than the original superconductor gap. This saturation of the topological gap can be ascribed to the absence of competition between the superconductor and the antiferromagnet. Including finite first neighbor interactions V_1 keeps the picture qualitatively unchanged, yet with a slightly renormalized topological gap (Fig. 4b). The interplay

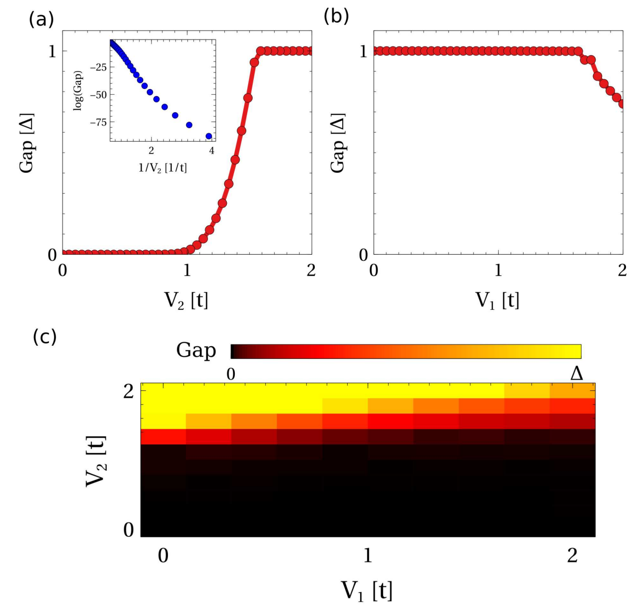

FIG. 4. (a) Evolution of the topological gap with the electron-electron interaction: (a) as a function of V_2 taking $V_1 = 0$, (b) as a function of V_1 taking $V_2 = 2t$. Panel (c) shows the topological gap as a function of the two electronic interactions V_1 and V_2, highlighting that only the second neighbor interaction opens up a gap. We took $\Delta = 0.2t$ and $m_{\mathrm{AF}} = 0.4t$.

between V_1 and V_2 shown in Fig. 4c shows that whereas V_2 opens the topological gap, V_1 leaves the system gapless or slightly renormalizes the topological gap. Finally, we note that imperfections and disorder are known to potentially impact topological superconductors by limiting the localization length and reducing the topological gap[63–65]. We verified that the phenomenology presented above is resilient towards Anderson disorder and happens for generic AF-SC interfaces[66]. Disorder slightly decreases the topological gap, yet without qualitatively impacting our results.

Finally, we address the potential experimental realization of our proposal. For a solid-state realization, no specific requirements are necessary for the superconductor besides conventional s-wave pairing, as realized in $NbSe_2$. The fundamental requirement is having a two-dimensional honeycomb antiferromagnetic insulator[67], as its electronic structure is expected to have the gapped Dirac points required for the emergence of the topological solitonic modes. Within van der Waals materials, trihalides host a magnetic honeycomb lattice[68], and in particular antiferromagnetic strained trihalides[69,70] would be suitable for our proposal. This pathway would require creating superconductor/antiferromagnet devices with those strained van der Waals materials. Within oxides, thin films of $InCu_{2/3}V_{1/3}\ O_3$[71] or β-$Cu_2V_2O_7$[72] has the required antiferromagnetic honeycomb lattice. For this possibility, a single layer of the bulk oxide should be epitaxially grown. Generic two-dimensional antiferromagnetic insulators hosting Dirac points in their normal state[73] would be suitable materials for our proposal, whose specific V_1, V_2 parameters can be inferred by first principles methods[74–77,78]. Finally, future ultracold atom setups[79] are potential platforms for the realization of our model, as honeycomb structures[80], antiferromagnetic correlations[81], long-range interactions[82–84] and s-wave correlations[85] in the normal state have been separately demonstrated. Interactions can be tuned from attractive to repulsive by magnetic fields; spatially dependent fields could be one way of creating the AF-SC interface, once superfluid correlations in a lattice have been reached.

To summarize, we have shown that an interface between a topologically trivial two-dimensional superconductor and antiferromagnetic insulator gives rise to a one-dimensional solitonic gas. Upon introduction of repulsive long-range interactions, we have demonstrated that a topological gap gets generated, giving rise to Majorana zero energy modes. The emergence of topological superconductivity appears in the absence of intrinsic spin-orbit coupling and is driven by repulsive Coulomb interactions. We showed that the topological gap appears at arbitrarily small interactions, and rapidly saturates to the gap of the parent superconductor, in stark contrast with conventional proposals involving competition between ferromagnetism and superconductivity. Our results propose a new mechanism to generate topological superconductivity based on interacting solitons, putting forward antiferromagnetic insulators as a potential materials platform for Majorana physics.

Acknowledgments: We acknowledge the computational resources provided by the Aalto Science-IT project. J. L. L. acknowledges financial support from the Academy of Finland Projects No. 331342 and No. 336243. P.T. acknowledges support by the Academy of Finland under project numbers 303351, 307419, and 327293.

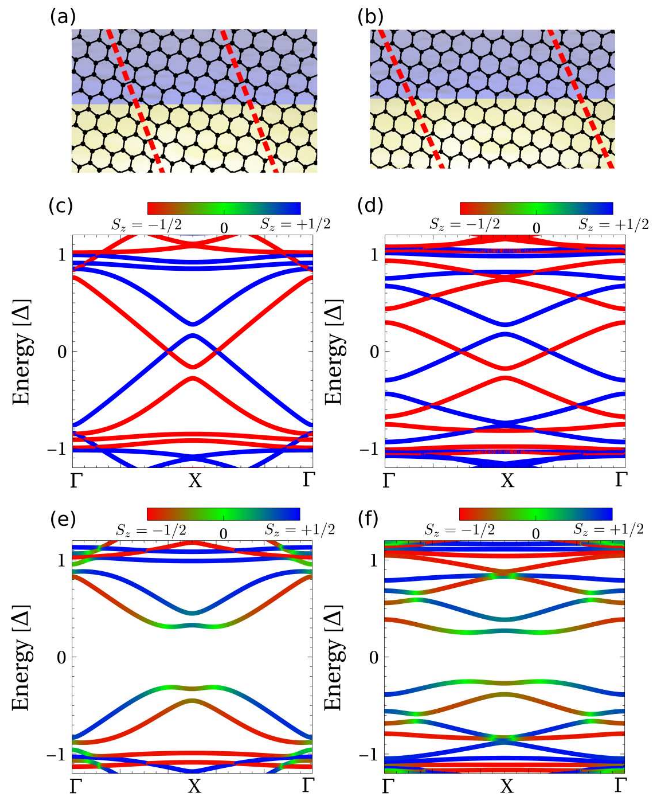

FIG. S5. (a,b) Sketch of two different interfaces, where dashed lines denote the size of the unit cell. Panels (c,d) show the non-interacting band-structures, featuring the solitonic interface modes. Panels (e,f) show the band-structures once interactions are included, showing the emergence of a topological gap. We chose $\Delta = 0.2t$, $m_{\text{AF}} = 0.4t$, and $V_2 = 1.7t$.

APPENDIX

In this Appendix, we show that an interaction-induced topological gap appears for generic interfaces (Sec. S1), we study the role of disorder on the topological gap (Sec. S2), analyze the microscopic origin of the interaction induced spin-orbit coupling (Sec. S3), and comment on real material estimates of the interaction (Sec. S4).

Appendix S1: Topological superconductivity in generic AF-SC interface

In the calculations included in the main manuscript, the orientation of the interface is the zigzag one. Here we show that generic orientations of the interface would work for our proposal. First, it is worth to mention that the emergence of the solitonic modes is not protected by a specific lattice symmetry, but they arise at the interface between inequivalently gapped Dirac equations. Those modes only appear when the antiferromagnet is in contact with the superconductor, and they are absent otherwise. The linear dispersion of the modes is then obtained by perturbation theory to the solitonic states. This phenomenology is expected to appear in generic interfaces, suggesting the emergent topological superconductivity does not depend on the details of the interface. In particular, we show in Fig. S5 the results for a heterostructure with two different non-zigzag interfaces. The specific structures are shown in Fig. S5ab, the non-interacting band-structures in Fig. S5cd, and the interacting mean-field band-structures in Fig. S5ef. In particular, it is observed that in the absence of interactions, the solitonic modes appear in generic interfaces. Furthermore, when interactions are included, a topological gap opens up for both interfaces. This phenomenology highlights the robustness of the solitonic modes to the details of the interface, and the generic emergence of a topological state driven by interactions.

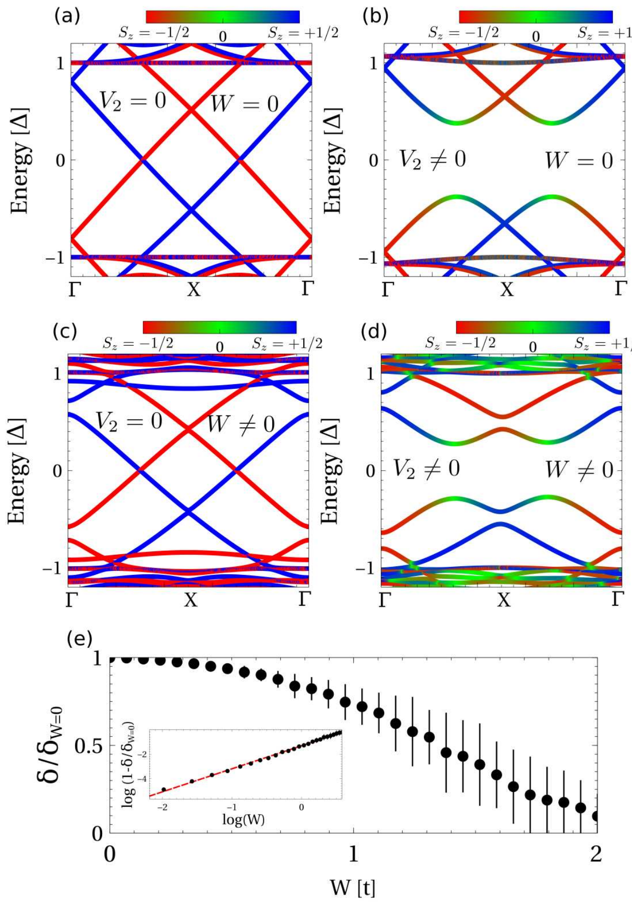

FIG. S6. (a,b) Band-structure for a supercell of size 5 in the absence of disorder (a,b) and in the presence of Anderson disorder $W = t$ (c,d). Panels (a,c) show the band-structure in the absence of interactions, and panels (c,d) in the presence of interactions. It is observed that the presence of disorder does not destroy the topological gap. Panel (e) shows the evolution of the ratio of the topological gap $\frac{\delta(W)}{\delta(W=0)}$ as a function of the disorder strength W, averaged over 100 disorder configurations for each W. The inset of (e) shows a log-log plot, highlighting the power-law behavior. We chose $\Delta = 0.2t$, $m_{\mathrm{AF}} = 0.4t$, and $V_2 = 1.7t$ in (b,d,e).

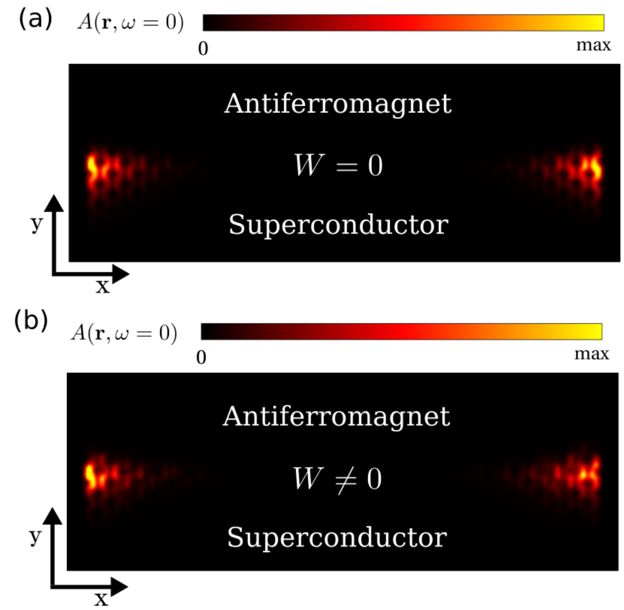

FIG. S7. Local density of states at zero energy for a finite slab without disorder (a) and with disorder $W = t$ (b). We observe that Majorana zero modes are present in both cases, highlighting the robustness of the topological state to Anderson disorder. We chose $\Delta = 0.2t$, $m_{\mathrm{AF}} = 0.4t$, and $V_2 = 1.7t$.

Appendix S2: Impact of disorder

The robustness to disorder is one of the crucial points of any proposal for Majorana states[63–65]. Since the fundamental physics of our proposal comes from the interface modes, for the sake of concreteness here we will in the following focus on disorder effects that affect the interface.

First, we address the impact of Anderson disorder in a periodic supercell in the $x-$direction. For this goal we take a supercell of 5 in the $x-$direction, include Anderson disorder by adding a term to the Hamiltonian of the form

$$\mathcal{H}_W = \sum_{i,s} W_i c^\dagger_{i,s} c_{i,s} \tag{S1}$$

where W_i is a random number between $[-W, W]$. The pristine case corresponds to taking $W = 0$. We show in Fig. S6 the comparison between the electronic structures with and without Anderson disorder in such supercell. In particular, for the pristine supercells we observe solitonic gapless modes in the absence of interactions (Fig. S6a), and a topological gap in the presence of interactions (Fig. S6b). To demonstrate the robustness of our phenomenology, we will consider a case with a relatively strong disorder $W = t$. When Anderson disorder is turned on, we observe than the solitonic modes remain mostly unaffected (Fig. S6c), and that in the presence of interactions, a topological gap remains (Fig. S6d). Interestingly, even with this strong disorder $W = t$, the topological gap keeps 73% percent of its pristine magnitude. The reduction of the topological gap as a function of the disorder is systematically explored in Fig. S6e. In particular, we observe that for a modest amount of disorder $W = 0.3t$, the topological gap keeps 97% of its pristine value. We have also performed a log-log plot of the gap reduction (inset of Fig. S6e), getting that the disorder dependence of the gap follows $\delta(W)/\delta(0) = 1-(W/W_C)^\gamma$ with $\gamma \approx 2$, where W_C is the critical disorder for the transition. The robustness of the topological state can be rationalized from its impact on the parent electronic structures. First, the s-wave superconducting state is resilient towards Anderson disorder as follows from Anderson's theorem[86,87]. The antiferromagnetic insulator is also robust to disorder due to its antiferromagnetic gap. And ultimately, the interface states are resilient to Anderson disorder due to their solitonic nature[49]. Finally, since the topological gap stems from an interaction-induced gap opening of the interface modes, the impact of the disorder on the topological gap is small due to the robustness of the solitonic modes.

Finally, we consider the effect of Anderson disorder in a large finite system, and in particular its impact on the Majorana zero-edge modes. For this sake, we now create a large system formed of 60 bulk cells in the $x-$direction, and we compute the density of states at zero energy. This is compared for the case without disorder $W = 0$, and for the case with Anderson disorder $W = t$, as shown in Fig. S7. We observe that in both cases, Majorana zero modes are located at the left and right ends of the interface. In particular, the persistence of zero modes in the disordered case highlights the robustness of the topological state towards Anderson disorder. Its origin can be rationalized as in the bulk case presented above.

Appendix S3: Interaction induced spin-orbit coupling

Here we comment on the specific form of the interaction-induced synthetic spin-orbit coupling. First, it is worth emphasizing that generically, onsite interactions U will also appear in the honeycomb model. These interactions are effectively included in our model at the mean-field level by means of the antiferromagnetic field. The existence of this antiferromagnetic order quenches any potential charge density wave orders or Haldane/Kane-Mele phases induced by V_1 and V_2. Therefore, both V_1 and V_2 do not have an impact on the bulk antiferromagnet, as the preexisting antiferromagnetic order quenches other emergent orders, but they only give rise to a finite effect on the interface states as they are originally gapless. Furthermore, we have explicitly verified that the emergent topological superconductivity also appears when a honeycomb lattice with U, V_1 and V_2 is solved at the mean-field level, with the antiferromagnetic field dynamically emerging from the selfconsistent solution.

The spin-orbit coupling term emerging from interactions in $\mathcal{H}^{MF}$ is related to the non-local terms $\chi_{ijss'}$ that involve second-neighbor hoppings and spin-flips. In particular, the term $\mathcal{H}^{MF}$ can be decomposed in its even and odd terms with respect to time-reversal symmetry. From the time-reversal symmetric component, we can extract the spin-dependent and spin-independent terms. In particular, we have verified that our self-consistent solution yields a spin-dependent time-reversal symmetric part of $\mathcal{H}^{MF}_{KM}$ that takes the form of a spatially-modulated Kane-Mele spin-orbit coupling[58] term of the form

$$\mathcal{H}^{MF}_{KM} = i \sum_{\langle\langle \alpha\beta \rangle\rangle} \sigma^y_{s,s'} \lambda \left(\frac{\mathbf{r}_\alpha + \mathbf{r}_\beta}{2} \right) \nu_{\alpha\beta} c^\dagger_{\alpha,s} c_{\beta,s'} \tag{S1}$$

so that

$$\chi^{KM}_{\alpha\beta ss'} = i\sigma^y_{s,s'} \lambda \left(\frac{\mathbf{r}_\alpha + \mathbf{r}_\beta}{2} \right) \nu_{\alpha\beta} \tag{S2}$$

where $\chi^{KM}_{\alpha\beta ss'}$ is the time-reversal symmetric, spin-dependent component of $\chi_{\alpha\beta ss'}$, $\langle\langle\rangle\rangle$ denotes second neighbors, $\nu_{\alpha\beta} = \pm 1$ for clock-wise and anticlockwise second-neighbor hopping, and $\lambda(\mathbf{r})$ is the spatial modulation strength of the selfconsistent profile. We have verified that this term is the one responsible for the gap opening in our system, whereas the rest of $\mathcal{H}^{MF}$ just creates small renormalizations in the band dispersion.

We now summarize the relation between the gap opening and the first and second neighbor interactions. The reason why V_2 is capable of opening a gap but not V_1 simply stems from the functional form of those solitonic modes. In particular, due to the original $U(1)$ spin symmetry of the system, gapping out the modes require creating spin-mixing between the two solitonic sectors. However, the interactions parametrized by V_1 that could give rise to spin-mixing yield mean-field single-particle terms that are zero when evaluated in the solitonic basis. This can be verified by explicitly adding a Rashba-like spin-orbit coupling term to the Hamiltonian (the interaction driven spin-mixing term that could appear from V_1), and observing that the interface modes remain gapless. In stark contrast, the interaction term parametrized by V_2 can potentially lead to a spin-mixing term of the Kane-Mele form, that when evaluated in the solitonic basis gives rise to a finite gap opening as explained above.

Appendix S4: Estimate of V_2 in real materials

Here we comment on the expected values of V_2 for real materials. First, it is worth to note that, as shown in our main manuscript, a strong $V_2 > t$ is not necessary for the topological phase to appear. Actually, we found that a topological gap appears for arbitrarily small V_2. Of course, the bigger the value of V_2, the bigger the topological gap would be.

In typical two-dimensional materials, second neighbor interactions are often comparable to the hopping. For example, in the case of graphene, second neighbor interaction is on the order of 4.2 eV[75]. This should be compared with the first neighbor hopping 3 eV, giving a ratio $V_2/t \approx 1.4$[75]. In the case of twisted two-dimensional materials, known to host correlated insulating states[88], this comparison can become more radical. For example, twisted graphene bilayers, whose effective model are also located in a honeycomb lattice[89], have second neighbor interactions on the same order as first neighbor ones[89]. A precise quantitative assessment of the second neighbor interaction in the candidate materials proposed in our main manuscript could be performed by exploiting recent developments in first-principles methods[74–77].

* jose.lado@aalto.fi
1 A Yu Kitaev, "Unpaired majorana fermions in quantum wires," Physics-Uspekhi **44**, 131–136 (2001).
2 Jason Alicea, "New directions in the pursuit of majorana fermions in solid state systems," Reports on Progress in Physics **75**, 076501 (2012).
3 C.W.J. Beenakker, "Search for majorana fermions in superconductors," Annual Review of Condensed Matter Physics **4**, 113–136 (2013).
4 Carlo Beenakker and Leo Kouwenhoven, "A road to reality with topological superconductors," Nature Physics **12**, 618–621 (2016).
5 M. T. Deng, C. L. Yu, G. Y. Huang, M. Larsson, P. Caroff, and H. Q. Xu, "Anomalous zero-bias conductance peak in a nb–InSb nanowire–nb hybrid device," Nano Letters **12**, 6414–6419 (2012).
6 A. D. K. Finck, D. J. Van Harlingen, P. K. Mohseni, K. Jung, and X. Li, "Anomalous modulation of a zero-bias peak in a hybrid nanowire-superconductor device," Phys. Rev. Lett. **110**, 126406 (2013).
7 Liang Fu and C. L. Kane, "Superconducting proximity effect and majorana fermions at the surface of a topological insulator," Phys. Rev. Lett. **100**, 096407 (2008).
8 Joel Röntynen and Teemu Ojanen, "Topological superconductivity and high chern numbers in 2d ferromagnetic shiba lattices," Phys. Rev. Lett. **114**, 236803 (2015).
9 Pavan Hosur, Pouyan Ghaemi, Roger S. K. Mong, and Ashvin Vishwanath, "Majorana modes at the ends of superconductor vortices in doped topological insulators," Phys. Rev. Lett. **107**, 097001 (2011).
10 Roman M. Lutchyn, Jay D. Sau, and S. Das Sarma, "Majorana fermions and a topological phase transition in semiconductor-superconductor heterostructures," Phys. Rev. Lett. **105**, 077001 (2010).
11 Jin-Peng Xu, Canhua Liu, Mei-Xiao Wang, Jianfeng Ge, Zhi-Long Liu, Xiaojun Yang, Yan Chen, Ying Liu, Zhu-An Xu, Chun-Lei Gao, Dong Qian, Fu-Chun Zhang, and Jin-Feng Jia, "Artificial topological superconductor by the proximity effect," Phys. Rev. Lett. **112**, 217001 (2014).
12 Gang Xu, Biao Lian, Peizhe Tang, Xiao-Liang Qi, and Shou-Cheng Zhang, "Topological superconductivity on the surface of fe-based superconductors," Phys. Rev. Lett. **117**, 047001 (2016).
13 Yasuhiro Asano and Yukio Tanaka, "Majorana fermions and odd-frequency cooper pairs in a normal-metal nanowire proximity-coupled to a topological superconductor," Phys. Rev. B **87**, 104513 (2013).
14 Qing Lin He, Lei Pan, Alexander L. Stern, Edward C. Burks, Xiaoyu Che, Gen Yin, Jing Wang, Biao Lian, Quan Zhou, Eun Sang Choi, Koichi Murata, Xufeng Kou, Zhijie Chen, Tianxiao Nie, Qiming Shao, Yabin Fan, Shou-Cheng Zhang, Kai Liu, Jing Xia, and Kang L. Wang, "Chiral majorana fermion modes in a quantum anomalous hall insulator–superconductor structure," Science **357**, 294–299 (2017).
15 F. Finocchiaro, F. Guinea, and P. San-Jose, "Topological π junctions from crossed andreev reflection in the quantum hall regime," Phys. Rev. Lett. **120**, 116801 (2018).
16 Michael Ruby, Falko Pientka, Yang Peng, Felix von Oppen, Benjamin W. Heinrich, and Katharina J. Franke, "End states and subgap structure in proximity-coupled chains of magnetic adatoms," Phys. Rev. Lett. **115**, 197204 (2015).
17 S. Nadj-Perge, I. K. Drozdov, J. Li, H. Chen, S. Jeon, J. Seo, A. H. MacDonald, B. A. Bernevig, and A. Yazdani, "Observation of majorana fermions in ferromagnetic atomic chains on a superconductor," Science **346**, 602–607 (2014).
18 S. M. Albrecht, A. P. Higginbotham, M. Madsen, F. Kuemmeth, T. S. Jespersen, J. Nygård, P. Krogstrup, and C. M. Marcus, "Exponential protection of zero modes in majorana islands," Nature **531**, 206–209 (2016).
19 M. T. Deng, S. Vaitiekėnas, E. B. Hansen, J. Danon, M. Leijnse, K. Flensberg, J. Nygård, P. Krogstrup, and C. M. Marcus, "Majorana bound state in a coupled quantum-dot hybrid-nanowire system," Science **354**, 1557–1562 (2016).
20 Jason Alicea, Yuval Oreg, Gil Refael, Felix von Oppen, and Matthew P. A. Fisher, "Non-abelian statistics and topological quantum information processing in 1d wire networks," Nature Physics **7**, 412–417 (2011).
21 Roger S. K. Mong, David J. Clarke, Jason Alicea, Netanel H. Lindner, Paul Fendley, Chetan Nayak, Yuval Oreg, Ady Stern, Erez Berg, Kirill Shtengel, and Matthew P. A. Fisher, "Universal topological quantum computation from a superconductor-abelian quantum hall heterostructure," Phys. Rev. X **4**, 011036 (2014).
22 V. Mourik, K. Zuo, S. M. Frolov, S. R. Plissard, E. P. A. M. Bakkers, and L. P. Kouwenhoven, "Signatures of majorana fermions in hybrid superconductor-semiconductor nanowire devices," Science **336**, 1003–1007 (2012).
23 Shawulienu Kezilebieke, Md Nurul Huda, Viliam Vaňo, Markus Aapro, Somesh C. Ganguli, Orlando J. Silveira, Szczepan Głodzik, Adam S. Foster, Teemu Ojanen, and Peter Liljeroth, "Topological superconductivity in a designer ferromagnet-superconductor van der Waals heterostructure," arXiv e-prints , arXiv:2002.02141 (2020), arXiv:2002.02141 [cond-mat.mes-hall].
24 Yuval Oreg, Gil Refael, and Felix von Oppen, "Helical liquids and majorana bound states in quantum wires," Phys. Rev. Lett. **105**, 177002 (2010).
25 Jay D. Sau, Roman M. Lutchyn, Sumanta Tewari, and S. Das Sarma, "Generic new platform for topological quantum computation using semiconductor heterostructures," Phys. Rev. Lett. **104**, 040502 (2010).
26 T. Jungwirth, X. Marti, P. Wadley, and J. Wunderlich, "Antiferromagnetic spintronics," Nature Nanotechnology **11**, 231–241 (2016).
27 V. Baltz, A. Manchon, M. Tsoi, T. Moriyama, T. Ono, and Y. Tserkovnyak, "Antiferromagnetic spintronics," Rev. Mod. Phys. **90**, 015005 (2018).
28 Ding-Fu Shao, Gautam Gurung, Shu-Hui Zhang, and Evgeny Y. Tsymbal, "Dirac nodal line metal for topological antiferromagnetic spintronics," Phys. Rev. Lett. **122**, 077203 (2019).
29 Wei Zhang, Matthias B. Jungfleisch, Wanjun Jiang, John E. Pearson, Axel Hoffmann, Frank Freimuth, and Yuriy Mokrousov, "Spin hall effects in metallic antiferromagnets," Phys. Rev. Lett. **113**, 196602 (2014).
30 Martin F. Jakobsen, Kristian B. Naess, Paramita Dutta, Arne Brataas, and Alireza Qaiumzadeh, "Electrical and thermal transport in antiferromagnet-superconductor junctions," Phys. Rev. B **102**, 140504 (2020).

[31] M. M. Otrokov, I. I. Klimovskikh, H. Bentmann, D. Estyunin, A. Zeugner, Z. S. Aliev, S. Gaß, A. U. B. Wolter, A. V. Koroleva, A. M. Shikin, M. Blanco-Rey, M. Hoffmann, I. P. Rusinov, A. Yu. Vyazovskaya, S. V. Eremeev, Yu. M. Koroteev, V. M. Kuznetsov, F. Freyse, J. Sánchez-Barriga, I. R. Amiraslanov, M. B. Babanly, N. T. Mamedov, N. A. Abdullayev, V. N. Zverev, A. Alfonsov, V. Kataev, B. Büchner, E. F. Schwier, S. Kumar, A. Kimura, L. Petaccia, G. Di Santo, R. C. Vidal, S. Schatz, K. Kißner, M. Ünzelmann, C. H. Min, Simon Moser, T. R. F. Peixoto, F. Reinert, A. Ernst, P. M. Echenique, A. Isaeva, and E. V. Chulkov, "Prediction and observation of an antiferromagnetic topological insulator," Nature **576**, 416–422 (2019).

[32] Chang Liu, Yongchao Wang, Hao Li, Yang Wu, Yaoxin Li, Jiaheng Li, Ke He, Yong Xu, Jinsong Zhang, and Yayu Wang, "Robust axion insulator and chern insulator phases in a two-dimensional antiferromagnetic topological insulator," Nature Materials **19**, 522–527 (2020).

[33] Chengwang Niu, Hao Wang, Ning Mao, Baibiao Huang, Yuriy Mokrousov, and Ying Dai, "Antiferromagnetic topological insulator with nonsymmorphic protection in two dimensions," Phys. Rev. Lett. **124**, 066401 (2020).

[34] Roger S. K. Mong, Andrew M. Essin, and Joel E. Moore, "Antiferromagnetic topological insulators," Phys. Rev. B **81**, 245209 (2010).

[35] Andreas Heimes, Panagiotis Kotetes, and Gerd Schön, "Majorana fermions from shiba states in an antiferromagnetic chain on top of a superconductor," Phys. Rev. B **90**, 060507 (2014).

[36] Aoyu Tan, Valentin Labracherie, Narayan Kunchur, Anja U. B. Wolter, Joaquin Cornejo, Joseph Dufouleur, Bernd Büchner, Anna Isaeva, and Romain Giraud, "Metamagnetism of weakly coupled antiferromagnetic topological insulators," Phys. Rev. Lett. **124**, 197201 (2020).

[37] Paul M. Sass, Jinwoong Kim, David Vanderbilt, Jiaqiang Yan, and Weida Wu, "Robust a-type order and spin-flop transition on the surface of the antiferromagnetic topological insulator $\mathrm{mnbi_2te_4}$," Phys. Rev. Lett. **125**, 037201 (2020).

[38] Kazushige Machida, Kazuo Nokura, and Takeo Matsubara, "Theory of antiferromagnetic superconductors," Phys. Rev. B **22**, 2307–2317 (1980).

[39] M. Weides, M. Disch, H. Kohlstedt, and D. E. Bürgler, "Observation of josephson coupling through an interlayer of antiferromagnetically ordered chromium," Phys. Rev. B **80**, 064508 (2009).

[40] J. W. A. Robinson, Gábor B. Halász, and M. G. Blamire, "Crossover induced by spin-density-wave interference in the coherence of singlet electron pairs in cr," Phys. Rev. Lett. **103**, 207002 (2009).

[41] C. Bell, E. J. Tarte, G. Burnell, C. W. Leung, D.-J. Kang, and M. G. Blamire, "Proximity and josephson effects in superconductor/antiferromagnetic $\mathrm{Nb}/\gamma-\mathrm{fe_{50}mn_{50}}$ heterostructures," Phys. Rev. B **68**, 144517 (2003).

[42] M. J. Nass, K. Levin, and G. S. Grest, "Bardeen-cooper-schrieffer pairing in antiferromagnetic superconductors," Phys. Rev. Lett. **46**, 614–617 (1981).

[43] Mark H. Fischer, Manfred Sigrist, and Daniel F. Agterberg, "Superconductivity without inversion and time-reversal symmetries," Phys. Rev. Lett. **121**, 157003 (2018).

[44] Sinisa Coh, Marvin L Cohen, and Steven G Louie, "Large electron–phonon interactions from FeSe phonons in a monolayer," New Journal of Physics **17**, 073027 (2015).

[45] Z. F. Wang, Huimin Zhang, Defa Liu, Chong Liu, Chenjia Tang, Canli Song, Yong Zhong, Junping Peng, Fangsen Li, Caina Nie, Lili Wang, X. J. Zhou, Xucun Ma, Q. K. Xue, and Feng Liu, "Topological edge states in a high-temperature superconductor FeSe/SrTiO3(001) film," Nature Materials **15**, 968–973 (2016).

[46] Taking a smooth transition between the superconductor and antiferromagnet does not impact the results qualitatively.

[47] Charge renormalization is reabsorbed in Eq. 2.

[48] M P Lopez Sancho, J M Lopez Sancho, J M L Sancho, and J Rubio, "Highly convergent schemes for the calculation of bulk and surface green functions," Journal of Physics F: Metal Physics **15**, 851–858 (1985).

[49] R. Jackiw and C. Rebbi, "Solitons with fermion number $\frac{1}{2}$," Phys. Rev. D **13**, 3398–3409 (1976).

[50] P. San-Jose, J. L. Lado, R. Aguado, F. Guinea, and J. Fernández-Rossier, "Majorana zero modes in graphene," Phys. Rev. X **5**, 041042 (2015).

[51] J. L. Lado and M. Sigrist, "Two-dimensional topological superconductivity with antiferromagnetic insulators," Phys. Rev. Lett. **121**, 037002 (2018).

[52] A. L. R. Manesco, G. Weber, and D. Rodrigues, "Effective model for majorana modes in graphene," Phys. Rev. B **100**, 125411 (2019).

[53] J. L. Lado and M. Sigrist, "Solitonic in-gap modes in a superconductor-quantum antiferromagnet interface," Phys. Rev. Research **2**, 023347 (2020).

[54] A. H. Castro Neto, F. Guinea, N. M. R. Peres, K. S. Novoselov, and A. K. Geim, "The electronic properties of graphene," Rev. Mod. Phys. **81**, 109–162 (2009).

[55] Jan Carl Budich and Eddy Ardonne, "Equivalent topological invariants for one-dimensional majorana wires in symmetry class d," Phys. Rev. B **88**, 075419 (2013).

[56] Details on the microscopic mean-field are included in the Supplemental Material.

[57] Zhenhua Qiao, Shengyuan A. Yang, Wanxiang Feng, Wang-Kong Tse, Jun Ding, Yugui Yao, Jian Wang, and Qian Niu, "Quantum anomalous hall effect in graphene from rashba and exchange effects," Phys. Rev. B **82**, 161414 (2010).

[58] C. L. Kane and E. J. Mele, "Quantum spin hall effect in graphene," Phys. Rev. Lett. **95**, 226801 (2005).

[59] C. Popovici, C. S. Fischer, and L. von Smekal, "Fermi velocity renormalization and dynamical gap generation in graphene," Phys. Rev. B **88**, 205429 (2013).

[60] T. Stauber, P. Parida, M. Trushin, M. V. Ulybyshev, D. L. Boyda, and J. Schliemann, "Interacting electrons in graphene: Fermi velocity renormalization and optical response," Phys. Rev. Lett. **118**, 266801 (2017).

[61] The term in $\mathcal{H}^{MF}$ creating the gap opening shows a similar exponential dependence.

[62] J. Bardeen, L. N. Cooper, and J. R. Schrieffer, "Theory of superconductivity," Phys. Rev. **108**, 1175–1204 (1957).

[63] Alejandro M. Lobos, Roman M. Lutchyn, and S. Das Sarma, "Interplay of disorder and interaction in majorana quantum wires," Phys. Rev. Lett. **109**, 146403 (2012).

[64] Niklas M. Gergs, Lars Fritz, and Dirk Schuricht, "Topological order in the kitaev/majorana chain in the presence of disorder and interactions," Phys. Rev. B **93**, 075129 (2016).

[65] İ. Adagideli, M. Wimmer, and A. Teker, "Effects of elec-

tron scattering on the topological properties of nanowires: Majorana fermions from disorder and superlattices," Phys. Rev. B **89**, 144506 (2014).
[66] Details on the role of Anderson disorder and different interfaces are provided in the Supplemental Material.
[67] Although square lattice models can have antiferromagnetism, their low energy model is usually not of the Dirac form.
[68] Michael McGuire, "Crystal and magnetic structures in layered, transition metal dihalides and trihalides," Crystals **7**, 121 (2017).
[69] Lucas Webster and Jia-An Yan, "Strain-tunable magnetic anisotropy in monolayer $crcl_3$, $crbr_3$, and cri_3," Phys. Rev. B **98**, 144411 (2018).
[70] Zewen Wu, Jin Yu, and Shengjun Yuan, "Strain-tunable magnetic and electronic properties of monolayer CrI3," Physical Chemistry Chemical Physics **21**, 7750–7755 (2019).
[71] A. Möller, U. Löw, T. Taetz, M. Kriener, G. André, F. Damay, O. Heyer, M. Braden, and J. A. Mydosh, "Structural domain and finite-size effects of the antiferromagnetic S = 1/2 honeycomb lattice in $incu_{2/3}v_{1/3}o_3$," Phys. Rev. B **78**, 024420 (2008).
[72] Alexander A. Tsirlin, Oleg Janson, and Helge Rosner, "β-$cu_2v_2o_7$: A spin-$\frac{1}{2}$ honeycomb lattice system," Phys. Rev. B **82**, 144416 (2010).
[73] T.O. Wehling, A.M. Black-Schaffer, and A.V. Balatsky, "Dirac materials," Advances in Physics **63**, 1–76 (2014).
[74] Priyanka Seth, Philipp Hansmann, Ambroise van Roekeghem, Loig Vaugier, and Silke Biermann, "Towards a first-principles determination of effective coulomb interactions in correlated electron materials: Role of intershell interactions," Phys. Rev. Lett. **119**, 056401 (2017).
[75] M. Schüler, M. Rösner, T. O. Wehling, A. I. Lichtenstein, and M. I. Katsnelson, "Optimal hubbard models for materials with nonlocal coulomb interactions: Graphene, silicene, and benzene," Phys. Rev. Lett. **111**, 036601 (2013).
[76] Iurii Timrov, Nicola Marzari, and Matteo Cococcioni, "Hubbard parameters from density-functional perturbation theory," Phys. Rev. B **98**, 085127 (2018).
[77] Iurii Timrov, Nicola Marzari, and Matteo Cococcioni, "Self-consistent Hubbard parameters from density-functional perturbation theory in the ultrasoft and projector-augmented wave formulations," arXiv e-prints , arXiv:2011.03271 (2020), arXiv:2011.03271 [cond-mat.mtrl-sci].
[78] A discussion on the V_2 values in two-dimensional materials is provided in the Supplemental Material.
[79] P. Törmä and K. Sengstock, *Quantum Gas Experiments – Exploring Many-Body States* (Imperial College Press, 2015).
[80] Gregor Jotzu, Michael Messer, Rémi Desbuquois, Martin Lebrat, Thomas Uehlinger, Daniel Greif, and Tilman Esslinger, "Experimental realization of the topological haldane model with ultracold fermions," Nature **515**, 237–240 (2014).
[81] Anton Mazurenko, Christie S. Chiu, Geoffrey Ji, Maxwell F. Parsons, Márton Kanász-Nagy, Richard Schmidt, Fabian Grusdt, Eugene Demler, Daniel Greif, and Markus Greiner, "A cold-atom fermi–hubbard antiferromagnet," Nature **545**, 462–466 (2017).
[82] S. Baier, M. J. Mark, D. Petter, K. Aikawa, L. Chomaz, Z. Cai, M. Baranov, P. Zoller, and F. Ferlaino, "Extended Bose-Hubbard Models With Ultracold Magnetic Atoms," Science **352**, 201–205 (2016).
[83] Elmer Guardado-Sanchez, Benjamin M. Spar, Peter Schauss, Ron Belyansky, Jeremy T. Young, Przemyslaw Bienias, Alexey V. Gorshkov, Thomas Iadecola, and Waseem S. Bakr, "Quench Dynamics of a Fermi Gas with Strong Long-Range Interactions," arXiv e-prints , arXiv:2010.05871 (2020), arXiv:2010.05871 [cond-mat.quant-gas].
[84] Bo Yan, Steven A. Moses, Bryce Gadway, Jacob P. Covey, Kaden R. A. Hazzard, Ana Maria Rey, Deborah S. Jin, and Jun Ye, "Observation of dipolar spin-exchange interactions with lattice-confined polar molecules," Nature **501**, 521–525 (2013).
[85] Debayan Mitra, Peter T. Brown, Elmer Guardado-Sanchez, Stanimir S. Kondov, Trithep Devakul, David A. Huse, Peter Schauß, and Waseem S. Bakr, "Quantum gas microscopy of an attractive fermi–hubbard system," Nature Physics **14**, 173–177 (2017).
[86] P.W. Anderson, "Theory of dirty superconductors," Journal of Physics and Chemistry of Solids **11**, 26–30 (1959).
[87] Lionel Andersen, Aline Ramires, Zhiwei Wang, Thomas Lorenz, and Yoichi Ando, "Generalized anderson's theorem for superconductors derived from topological insulators," Science Advances **6**, eaay6502 (2020).
[88] Yuan Cao, Valla Fatemi, Ahmet Demir, Shiang Fang, Spencer L. Tomarken, Jason Y. Luo, Javier D. Sanchez-Yamagishi, Kenji Watanabe, Takashi Taniguchi, Efthimios Kaxiras, Ray C. Ashoori, and Pablo Jarillo-Herrero, "Correlated insulator behaviour at half-filling in magic-angle graphene superlattices," Nature **556**, 80–84 (2018).
[89] Mikito Koshino, Noah F. Q. Yuan, Takashi Koretsune, Masayuki Ochi, Kazuhiko Kuroki, and Liang Fu, "Maximally localized wannier orbitals and the extended hubbard model for twisted bilayer graphene," Phys. Rev. X **8**, 031087 (2018).